nature photonics

Article

https://doi.org/10.1038/s41566-024-01455-6

Multicolour stretchable perovskite electroluminescent devices for user-interactive displays

Received: 26 April 2023

Accepted: 26 April 2024

Published online: 4 June 2024

Check for updates

Fengjun Chun[1,4], Binbin Zhang[2,4], Yuyu Gao[2,4], Xiaohe Wei[1], Qiang Zhang[2], Weilin Zheng[1], Jingkun Zhou[2], Yang Guo[1], Xin Zhang[1], Zhifeng Xing[1], Xinge Yu[2] ✉ & Feng Wang[1,3] ✉

Wearable displays require mechanical deformability to conform to the skin, as well as long-term stability, multicolour emission and sufficient brightness to enable practically useful applications. However, endowing a single device with all the features remains a challenge. Here we present a rational material design strategy and simple device-manufacturing process for skin-conformable perovskite-based alternating-current electroluminescent (PeACEL) devices. These devices exhibit a narrow emission bandwidth (full-width at half-maximum, <37 nm), continuously tuneable emission wavelength (468–694 nm), high stretchability (400%) and adequate luminance (>200 cd m^{-2}). The approach leverages a new class of perovskite zinc sulfide (PeZS) phosphors, consisting of ZnS phosphors coated with perovskite nanoparticles for electrical excitation via total intraparticle energy transfer. This strategy results in pure red and green emissions and expands the colour gamut of powder-based ACEL devices by 250%. Moreover, our processing technique facilitates the integration of PeACEL displays with wearable electronics, enabling applications in dynamic interactive displays and visual real-time temperature monitoring. These PeACEL displays offer new routes in flexible electronics and hold potential for the development of efficient artificial skins, robotics and biomedical monitoring devices.

Wearable electronics featuring mechanical deformability and multi-faceted intelligent capabilities have experienced rapid progress and witnessed extensive impact on our daily life[1–5]. Visual displays, as the core component, have emerged as the primary medium of information dissemination. Wearable displays possess distinct advantages, such as flexibility or even stretchability, portability, deformability and skin conformability, thereby enhancing convenience and comfort[6–10]. Various display technologies have been developed, including liquid crystal displays (LCDs), organic light-emitting diodes (OLEDs), quantum dot light-emitting diodes (QLEDs), perovskite light-emitting diodes (PeLEDs) and alternating-current electroluminescent (ACEL) devices (Fig. 1a)[11–15]. Non-self-emissive LCDs are the workhorse for contemporary display technology due to their long lifetime, resolution, cost-effectiveness and brightness. Nevertheless, the rigidity of colour filters and backlight sources (light-emitting diodes) severely limits the flexibility of LCDs. In recent years, self-emissive displays

[1]Department of Materials Science and Engineering, City University of Hong Kong, Hong Kong SAR, China. [2]Department of Biomedical Engineering, City University of Hong Kong, Hong Kong SAR, China. [3]Hong Kong Institute for Clean Energy, City University of Hong Kong, Hong Kong SAR, China. [4]These authors contributed equally: Fengjun Chun, Binbin Zhang, Yuyu Gao. ✉e-mail: xingeyu@cityu.edu.hk; fwang24@cityu.edu.hk

https://doi.org/10.1038/s41566-024-01455-6

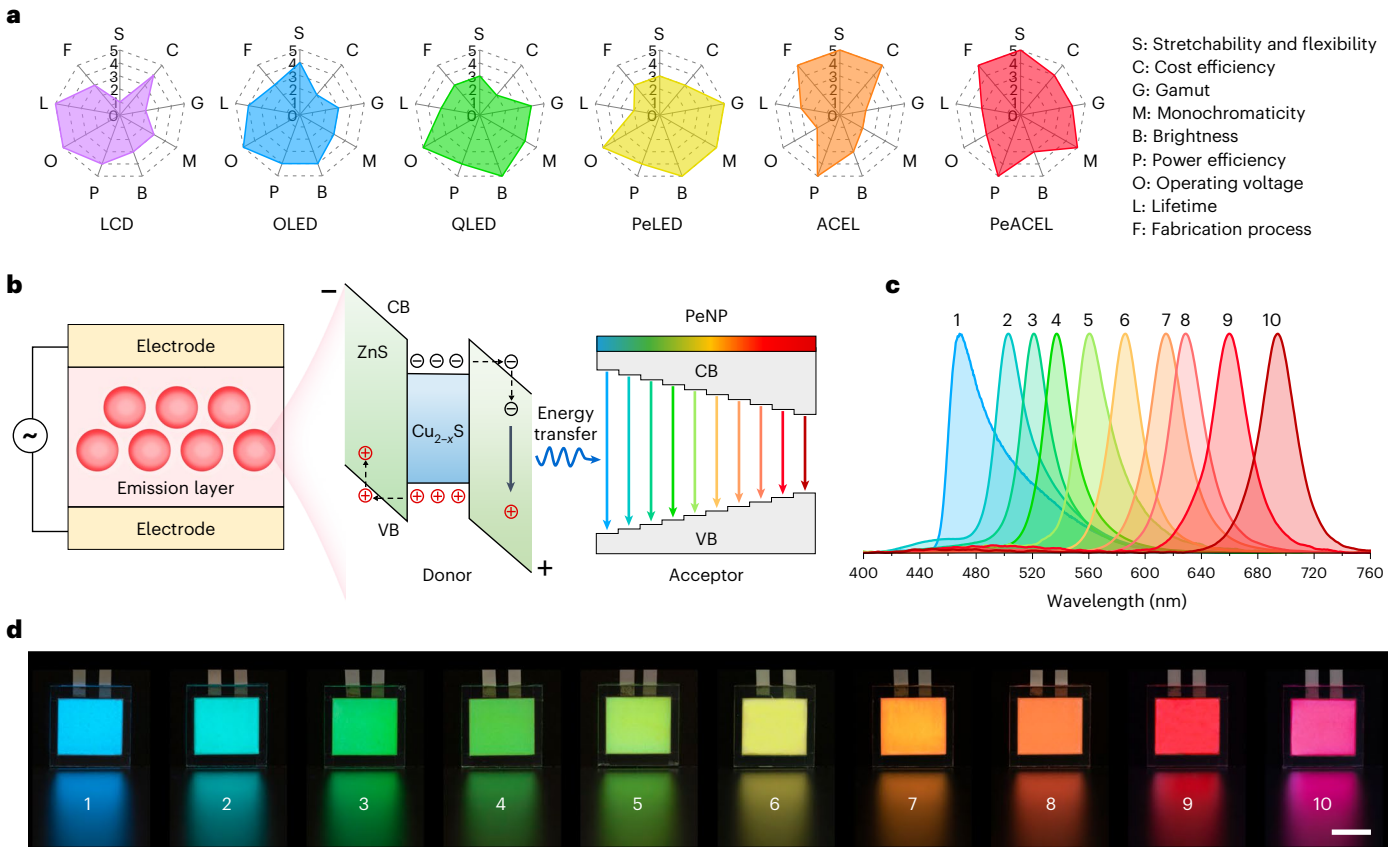

Fig. 1 | Colour-tuneable PeACEL device. a, Comparison of performance merits of current display technologies, including LCDs, OLEDs, QLEDs, PeLEDs, ACEL and PeACEL devices. **b**, Working mechanism of the PeACEL device. **c**,**d**, EL spectra (**c**) and photographs (**d**) of full-colour PeACEL devices operating at 100 V, 20 kHz. Scale bar, 1 cm. CB and VB represent the conduction band and valence band, respectively.

(OLEDs, QLEDs and PeLEDs) have witnessed considerable advances, particularly in terms of the wider colour gamut, more vivid colour and better flexibility[16–22]. Yet, their intrinsic instability of emitting materials necessitates stringent environmental control, such as an inert gas atmosphere, humidity and temperature. Additionally, these devices impose strict requirements on the electrode work functions to achieve balanced charge injection. Such high dependency on equipment and material significantly elevates the fabrication cost and complexity.

In contrast, the ACEL device has been explored as a viable contender to evolve wearable displays, owing to its simple manufacturing, superior deformability, low power consumption and long lifetime[23]. However, the limited colour capabilities and high driving alternating voltages of ACEL are perceived as major obstacles to practical applications[24]. Commercial ACEL phosphors exhibit broad full-width at half-maximum (FWHM) of >50 nm and a confined colour region from blue to orange, implying poor colour purity and a restricted colour gamut (Supplementary Fig. 1). Furthermore, the electroluminescence (EL) performance of orange-emitting phosphors is markedly inferior to blue- and green-emitting phosphors, thereby impeding the monolithic integration of full-colour displays. Lead halide perovskite nanoparticles (PeNPs) have been proposed as a promising colour conversion layer for flexible pure-colour ACEL devices owing to their high absorption coefficients, high photoluminescence quantum yield, tuneable emission spectra and narrow FWHM[25,26]. Nonetheless, challenges persist in achieving ultrathin, stretchable, large-area and colourful displays for wearable electronics, primarily due to the intricate multilayer phosphor package structure. Besides, the requirement of high driving voltages to attain sufficient brightness presents an additional hurdle for the realization of wearable applications.

Here we describe a full-colour perovskite-based alternating-current electroluminescent (PeACEL) device with high colour purity, brightness, flexibility and stretchability. We develop a new class of EL phosphors composed of PeNPs-coated ZnS (PeZS) for the effective electrical excitation of PeNPs through total intraparticle energy transfer. The EL spectra of PeACEL devices can be tuned from blue to deep red (468–694 nm) with a narrow FWHM (<37 nm), and the brightness (>500 cd m^{-2}) is comparable with that of commercial planar displays (100–300 cd m^{-2}) (ref. 23). Ultrathin (95 µm) and extremely stretchable (400%) PeACEL devices with double-sided light emission were fabricated using silver nanowires (AgNWs) as the transparent electrode. Demonstrations showcased that the integration of these flexible PeACEL displays with soft electronics enables various smart functionalities, including user-interactive skin displays and intelligent soft robotics, that convert sensory signals into visual feedback, thereby providing a more efficient and intuitive information transmission method.

Results

Design of full-colour PeACEL device

The standard architecture of powder-type ACEL devices is characterized by an emission layer (EML) sandwiched between two electrodes, with at least one electrode being transparent. The ACEL phosphors are well embedded in a polymer matrix to constitute the EML. Commercial ACEL phosphors primarily consist of ZnS doped with various elements (such as Cu, Al and Mn), and the EL lighting can be tuned from blue to orange by modulating the dopant composition[27]. However, the scarcity of high-colour-purity phosphors and red-emitting phosphors (>610 nm) remains an impediment to achieve a full-spectrum display. In this work, we developed a class of colour-tuneable PeZS phosphors

https://doi.org/10.1038/s41566-024-01455-6

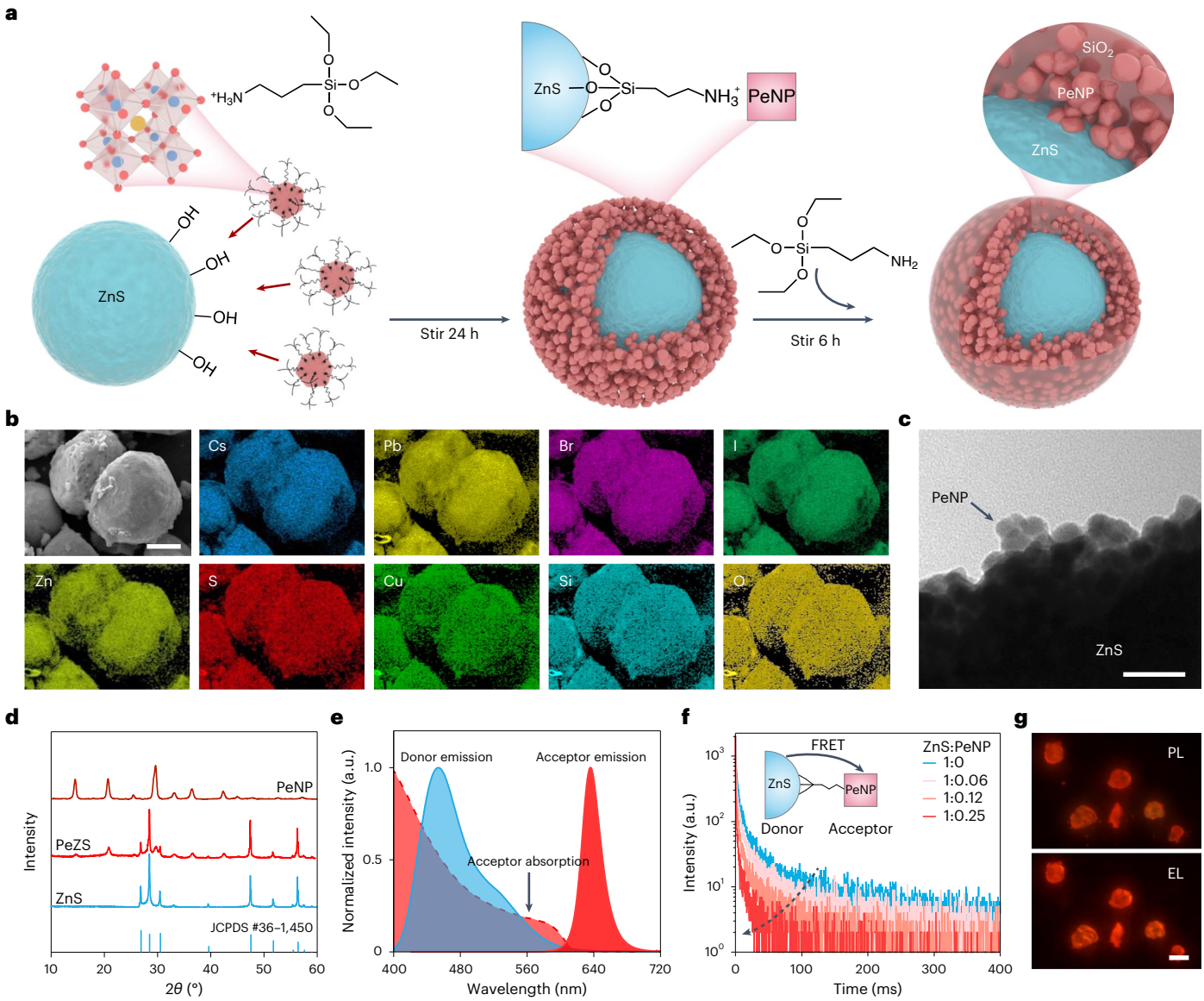

Fig. 2 | Synthesis and characterization of PeZS phosphors. a, Schematic of the fabrication process. **b**, Scanning electron microscopy images and energy-dispersive X-ray spectroscopic mapping of red-emitting PeZS phosphors. Scale bar, 10 μm. **c**, TEM image of red-emitting PeZS phosphors. Scale bar, 50 nm. **d**, XRD pattern. **e**, Absorption and emission spectra of PeNPs (red) and commercial ZnS (blue). **f**, Decay curves of PeZS with increasing PeNPs ratio (λ_{exc} = 370 nm, λ_{em} = 500 nm). The dashed arrow indicates the gradually decreasing average lifetime of PeZS phosphors with an increase in PeNPs loading. The inset shows a schematic of the FRET from ZnS to PeNPs. **g**, Optical micrograph of individual PeZS particles under UV light (top) and a.c. electric field (bottom) excitation. Scale bar, 20 μm.

by combining blue ZnS phosphors and PeNPs. The composite phosphors integrate electrical excitation and total energy transfer at the single-particle level, rendering full-spectrum emission from the PeNPs in an electrical field (Fig. 1b). Specifically, the ZnS core particle is first electrically excited due to intrinsic heterojunctions within the crystal[6]. Next, the excitation energy generated in the core layer is extracted by the PeNP shell through the combined effects of photon reabsorption and Förster resonance energy transfer (FRET). Finally, light emission from the PeNP shell concurrently renders high colour purity and spectral tunability (468–694 nm) (Fig. 1c,d).

The formation process of the PeZS phosphors is depicted in Fig. 2a. $CsPbX_3$ (X = Cl, Br, I) nanoparticles were synthesized using the modified hot injection method. The branched capping ligand, (3-aminopropyl) triethoxysilane (APTES), was employed to prepare the PeNPs as the passivator and stabilizer[28,29]. APTES-modified PeNPs with different halide compositions show tuneable emission colour and uniform size distribution (Supplementary Fig. 2). Contrary to previous reports, immediate cleaning was required to avert the further in situ hydrolysis of the silicone capping agent, which otherwise would form a thick coating layer on the PeNPs surface. The washed PeNPs were rapidly mixed with pristine ZnS, enabling the direct attachment of APTES-modified PeNPs to the surface of ZnS via the reaction between the silyl ether ($-SiOC_2H_5$) functional groups of APTES and the hydroxyl group of ZnS (Supplementary Fig. 3). Subsequently, additional APTES was introduced into the reaction solution to enhance environmental stability. The $-SiOC_2H_5$ groups of APTES were hydrolysed to form a Si–O–Si cross-linked matrix that enveloped the surface of the PeZS phosphors. Using this method, we successfully obtained a series of colour-tuneable PeZS phosphors with highly monochromatic emission (Supplementary Fig. 4). To verify the composition of PeZS phosphors, energy-dispersive X-ray spectroscopic mapping was conducted. As displayed in Fig. 2b, all the elements of ZnS and red PeNPs (Cs, Pb, Br, I, Zn, S, Cu, Si and

O) were detected, and the uniform distribution indicated the PeNPs are densely coated on the surface of ZnS. The transmission electron microscopy (TEM) and high-resolution TEM images reveal that several layers of PeNPs were attached to the ZnS surface, with PeNPs uniformly encased within the SiO_2 matrix (Fig. 2c and Supplementary Fig. 5). The SiO_2 presence is confirmed by the bands at 1,112 and 1,028 cm^{-1} in the Fourier transform infrared spectra, which are assigned to Si–O–Si and Si–O–C (Supplementary Fig. 6)[29].

The X-ray diffraction patterns of ZnS, PeNPs and PeZS are illustrated in Fig. 2d and Supplementary Fig. 7a. The XRD pattern of PeZS corroborated the presence of the hexagonal ZnS structure and cubic $CsPbX_3$ structure, with the major peak positions remaining constant. In particular, the diffraction peak intensity of ZnS appreciably diminished, implying the formation of a dense PeNP coating layer on the particle surface that attenuated the X-ray photons. Furthermore, the broad diffraction peak ranging from 15° to 35° confirms the formation of the SiO_2 protective layer.

The core–shell particle configuration is beneficial for energy transfer from ZnS to PeNPs that display sufficient spectral overlaps (Fig. 2e and Supplementary Fig. 7b). On one hand, the PeNP coating layer can capture light emissions from the ZnS core in all directions. On the other hand, the structure promised close proximity between ZnS and PeNPs for FRET to proceed[30], which was confirmed by time-decay studies (Fig. 2f, Supplementary Figs. 8 and 9 and Supplementary Note 1). Specifically, the average lifetime of PeZS phosphors progressively decreased from 21.09 to 6.32 ms with a gradual increase in PeNPs loading, suggesting a great contribution of FRET to the overall energy transfer process. The efficient FRET observed in the microsized phosphors was ascribed to the presence of numerous diminutive luminescence centres within ZnS (ref. 31), which could form an energy migration network to bridge energy transfer over an extended distance[30,32].

The hierarchical material structure enables efficient light emissions with high colour purity at the single-particle level by photon and electrical excitations (Fig. 2g and Supplementary Fig. 10a,b). In control experiments involving physically mixed ZnS and PeNPs, the leakage of blue light was preserved even in the presence of an excessive amount of PeNPs, owing to the reduced photon absorption and the absence of FRET (Supplementary Figs. 10c,d, 11 and 12). Single-particle emission will also endow PeZS-based EL devices with superior performance compared with their counterparts consisting of an additional conversion layer, primarily in ensuring emission uniformity, diminishing device thickness, enhancing material utilization and attaining high luminance (Supplementary Figs. 13 and 14 and Supplementary Note 2). On a separate note, the as-synthesized PeZS phosphors exhibit exceptional stability against moisture, thereby laying a foundation for durable EL devices (Supplementary Figs. 15 and 16 and Supplementary Note 2).

EL performance of PeACEL device

The PeACEL device was first assessed using a typical sandwich structure (Fig. 1b), which consists of a transparent electrode (indium tin oxide), an EML (PeZS and $BaTiO_3$ dispersed in polydimethylsiloxane (PDMS)) and another silver electrode (Supplementary Fig. 17). Figure 3a depicts the narrowband emission of the PeACEL devices with FWHM of 37 nm (blue), 24 nm (green) and 29 nm (red), as well as nearly undetectable emission from the ZnS donor. In contrast, the EL bandwidth of commercial blue (66 nm), green (81 nm) and orange (56 nm) ACEL are much broader (Fig. 3a). By virtue of their ultrahigh colour purity, the PeACEL devices substantially expand the colour gamut of ZnS-based ACEL by 2.1 fold (Fig. 3b). In alliance with blue commercial ZnS, the colour gamut can be further expanded (2.5 fold).

Another feature of the PeACEL device is its high frequency stability against colour drift. Commercial blue and green ZnS phosphors are frequency-dependent materials[31,33], exhibiting an emission colour shift as the operating frequency increases from 100 Hz to 20 kHz (Fig. 3c and Supplementary Fig. 18). Given its sensitivity to frequency, increasing the operating voltage is the only way to achieve a bright, specific colour. For instance, to generate green light emission, one must operate at a low-frequency level (≤500 Hz). By comparison, the spectral shape and peak position of PeACEL devices are completely independent of frequency (Fig. 3d and Supplementary Fig. 19). The observation highlights the near-unity intraparticle energy transfer within the PeACEL devices, which combine the roles of both FRET effect and broadband absorption.

The luminance of the PeACEL and ACEL devices against the applied voltage and frequency was tested (Fig. 3e and Supplementary Fig. 20). The luminance of all the devices displayed a positive correlation with voltage and frequency. In particular, the performance of blue-, green- and red-emitting PeACEL devices is comparable with that of the blue-emitting ACEL device (>500 cd m^{-2} at 200 V, 20 kHz), owing to the high energy conversion efficiency, low photon loss and unaltered electric field strength of the PeACEL device (Fig. 3f and Supplementary Note 2). The luminance of green and red PeACEL devices even outperforms the corresponding ACEL devices under the same operating voltage. Through a parallel comparison of the devices, it was found that the red PeACEL device exhibits a lower turn-on voltage (<25 V) and higher brightness (4.1 times) than the orange ACEL device (Fig. 3f and Supplementary Fig. 21a,b). In addition, we also demonstrated that the red PeACEL device ($V_{a.c.}$ = 100 V, $f_{a.c.}$ = 20 kHz) achieves a brightness of 147 cd m^{-2}, which is sufficient to illuminate a paper-based document (Supplementary Fig. 21c).

Response time is also crucial for display applications, and PeACEL devices achieve a fast response at the level of hundreds of microseconds (Supplementary Fig. 22 and Supplementary Table 1). The storage and operational stabilities of the PeACEL devices were assessed by measuring the luminance and peak positions of their EL spectra. Following a 60-day testing period (100 V, 20 kHz, 2 h daily duty circle), the EL luminance of the blue, green and red PeACEL devices sustained above 88%, and no shift in the emission peak was observed (Fig. 3g,h). Moreover, the devices demonstrated exceptional stability throughout a continuous operation span of 360 h, whereas the luminance of the devices employing uncoated ZnS phosphors exhibited a pronounced decline (Supplementary Fig. 23). A reduction in the operational frequency has been identified as a potential approach to further extend the longevity of the devices (Supplementary Fig. 24). The outstanding operational stability of PeACEL devices can be attributed to the synergetic effects of the physical barriers and the inherent characteristics of a.c. operation. The polymer matrix, coupled with the protective SiO_2 overcoat, establishes a dual-layer defence mechanism that effectively impedes the ingress of moisture and oxygen, thereby safeguarding the core ZnS and PeNPs against degradation (Supplementary Note 2). Unlike their d.c.-driven counterparts, the frequent reversal of the electric field in PeACEL devices can effectively inhibit ion migration caused by charge accumulation. Additionally, much less heat generation of the PeACEL devices further minimizes the risk of perovskite thermal degradation.

Stretchable PeACEL device

The schematic of the stretchable PeACEL device is represented in Fig. 4a. AgNWs with large aspect ratios were spray coated on pre-strained styrene–ethylene–butylene–styrene (SEBS) substrates as transparent stretchable electrodes. The EML was fabricated by combining the elastomer (SEBS) with blue, green and red PeZS phosphors. It was observed that the PeZS phosphors were evenly distributed within the SEBS matrix (Supplementary Fig. 25). Operating at 200 V/20 kHz, the luminance of the blue, green and red stretchable devices reached 227, 254 and 276 cd m^{-2}, respectively (Supplementary Fig. 26a). As shown in Fig. 4b, these operating devices maintain bright emission up to a considerable strain of 400%, and this ultrahigh stretchability benefits from the pre-strain approach and the intrinsic properties of SEBS (Supplementary Fig. 27). The luminance of red-emitting PeACEL devices, as a function of elongation, is illustrated in Fig. 4c. The brightness of the

https://doi.org/10.1038/s41566-024-01455-6

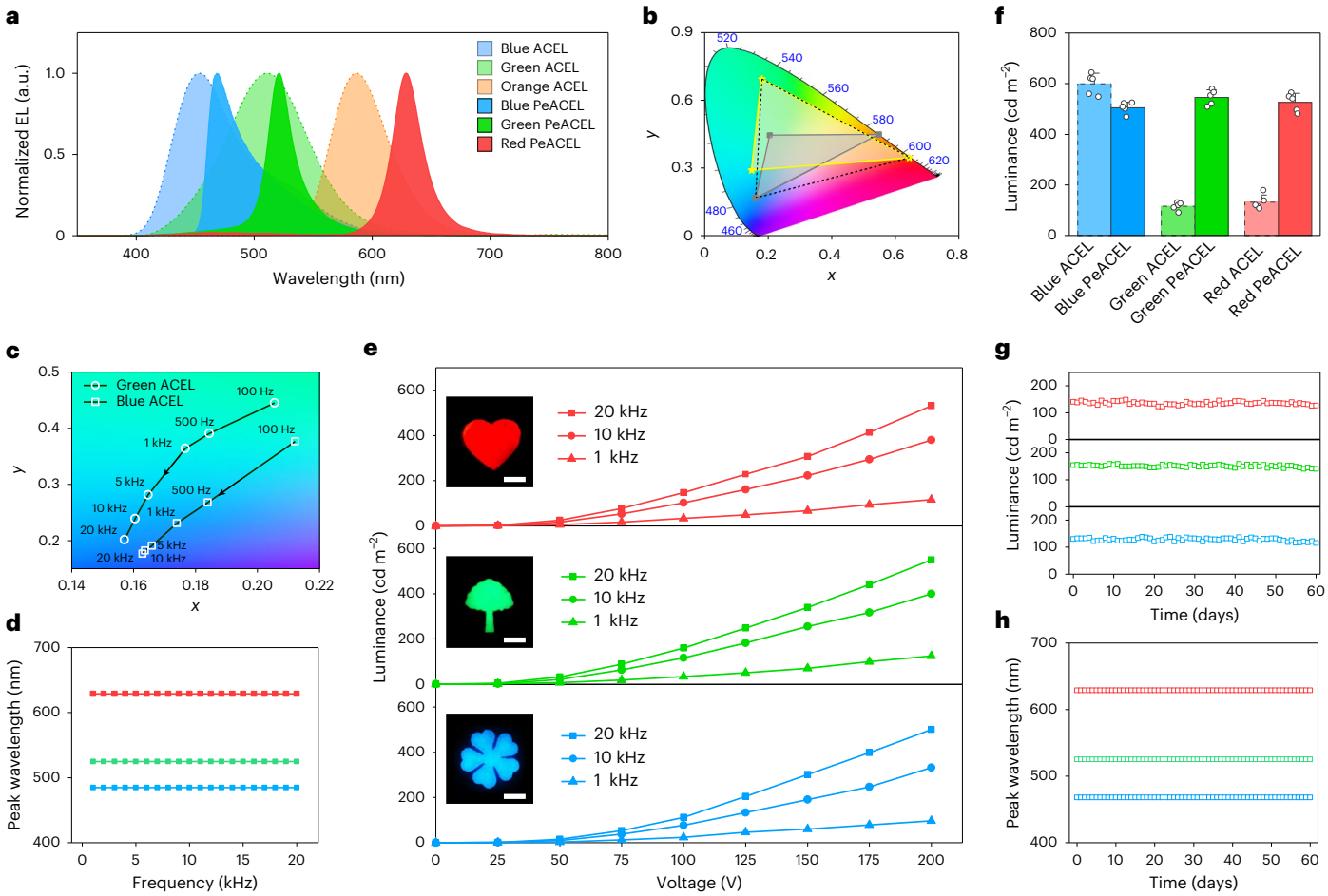

Fig. 3 | EL performance of PeACEL devices. a, EL spectra of blue, green and red PeACEL and ACEL devices. **b**, CIE coordinates of ACEL (grey square) and PeACEL (yellow star) devices. The black dashed lines indicate that a wider colour gamut can be achieved by combining green and red PeZS with blue commercial ZnS. **c**, CIE coordinates of the frequency-dependent blue and green ACEL devices. **d**, Evolution of the peak position of EL as a function of frequency. **e**, Luminance–voltage curves. The insets show the EL images of the patterned devices. Scale bars, 1 cm. **f**, Comparison of the luminance of PeACEL and ACEL devices at 200 V and 20 kHz. Note that the green ACEL operates at 500 Hz due to its frequency sensitivity. Bar height, mean; error bars, standard deviation; $n = 5$ independent devices. **g**, Evaluation of storage and operational stability over a 60-day period, with the devices undergoing a daily operation of 2 h. **h**, Peak position of the EL spectra across different days.

PeACEL device shows an enhancement as the strain increases to 300%, subsequently followed by a mild decrement, which is attributed to the alterations in the electric field and the density of light-emitting particles during the stretching process (Supplementary Note 3). Figure 4d shows the plot of the normalized EL intensity of the operating PeACEL device after 500 cycles of 100% elongation. The EL intensity fluctuations during cyclic stretching are fully reversible without significant changes. The cross-sectional view of the stretchable device in the unstretched state reveals a total thickness of 95 µm, with PeZS embedded in the SEBS matrix (Fig. 4e). The ultrathin PeACEL device can endure considerable and repeated tensile deformations, which are ideal for use in wearables. Moreover, the long-term stability and sufficient brightness further underscore its impressive application prospects (Supplementary Fig. 26b).

The facilitation of patterned displays is essential for wearable electronics. To this end, we fabricated eight patterned PeACEL devices with various emitting colours, utilizing a consistent structure. Four Chinese characters (winter, spring, autumn and summer) and four distinct animals (polar bear, rabbit, tiger and panda) were employed, each corresponding to one of the four emitting colours (blue, green, yellow and red), respectively. These patterned devices are deformable and stretchable under operational conditions (Fig. 4f and Supplementary Fig. 28). Besides, the implementation of double-sided transparent electrodes enables these devices to exhibit double-sided light emission, offering advantages for specific applications (Supplementary Fig. 29). Achieving such high stretchability, high colour purity and ultrathinness and ease of patterning in a single ACEL device is indeed unprecedented. Although employing an additional colour conversion layer is also capable of achieving high colour purity and using hydrogels as electrodes can offer higher stretchability, the intrinsic characteristics of these alternative designs pose challenges in realizing ultrathin and patterned devices (Supplementary Figs. 30 and 31 and Supplementary Table 2).

User-interactive skin display integration

User-interactive electronic skin with an intuitive signal display holds tremendous potential for emerging human–machine interfaces, artificial skin and health-monitoring systems[34–36]. These interactive displays are endowed with a variety of smart functions, derived from the integration of flexible display elements and stimulus-responsive sensors (that is, pressure, temperature, strain and chemical stimuli)[37,38]. Here ultrathin, lightweight, skin-deformable, durable and multicolour displays are indispensable components. We demonstrate two smart skin displays with interactive functionality, using the PeACEL devices that meet the aforementioned criteria. The PeACEL devices demonstrate a robust instantaneous visual response in terms of pattern or

https://doi.org/10.1038/s41566-024-01455-6

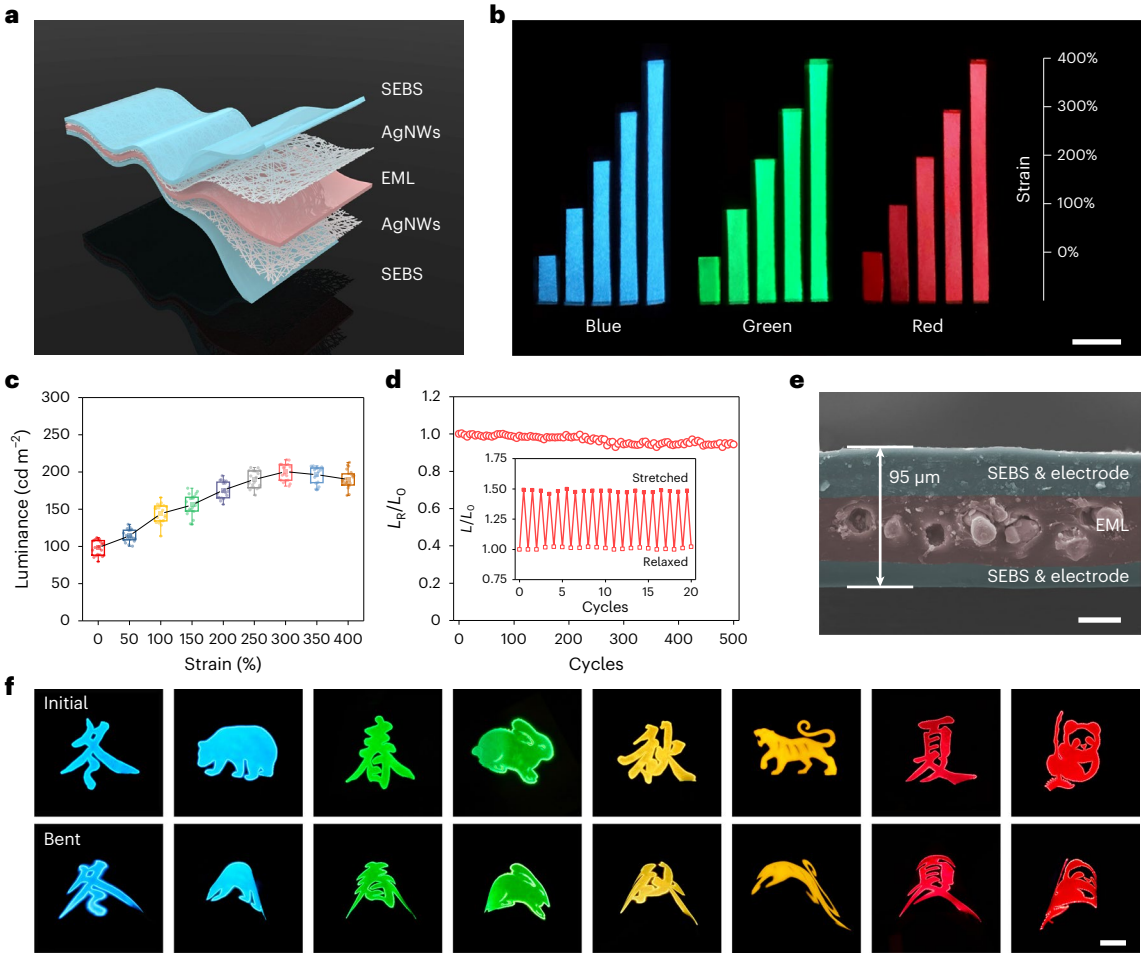

Fig. 4 | Flexible and stretchable PeACEL devices operating at 100 V, 20 kHz. **a**, Schematic of the stretchable PeACEL device, which comprises PeZS phosphors embedded in SEBS as the EML and AgNW networks encased within SEBS as the electrodes. **b**, EL images of the activated PeACEL devices being subjected to various levels of strain. Scale bar, 1.5 cm. **c**, Dependence of the luminance of PeACEL devices on strains. Ten devices were used in the test, with each device being tested twice. Squares, mean; box limits, upper and lower quartiles; whiskers, 1.5× interquartile range; points, outliers; $n = 20$ independent spots. **d**, Mechanical stability test of the PeACEL device for 500 cycles. The inset shows the relative intensity under the relaxed and stretched states with 100% strain for the initial 20 cycles. **e**, Cross-sectional view of the device. Scale bar, 30 μm. **f**, EL images of the patterned PeACEL devices at the initial (top) and bent (bottom) states. Scale bar, 1 cm. L_0 represents the initial luminance without any strain, L_R stands for the luminance when the device is relaxed during stretching cycles and L denotes the luminance at 100% strain and on returning to the relaxed state.

colour transformation, facilitating effective information dissemination (Fig. 5a). Figure 5b illustrates the system-level overview of power supply, signal acquisition, analysis, transduction and processing to facilitate the skin-integrated dynamic interactive display, where a rationally designed circuit is equipped to maintain user safety (Supplementary Fig. 32 and Supplementary Note 4). Moreover, biocompatibility testing indicates that the PeACEL device is non-toxic and can be directly applied to the skin (Supplementary Fig. 33).

As shown in Fig. 5c, the skin-integrated red PeACEL array of individually controllable pixels could dynamically display desired patterns (shaped to form the letters 'REDPEACEL'). To demonstrate the application potential of smart displays, a user-interactive display involving the multipixel array of individually addressable PeACEL and a laser-induced graphene (LIG)-based tactile sensor was constructed and mounted on the user's arm and hand (Supplementary Fig. 34). The on-skin tactile sensor with high sensitivity and instant response served as a control panel to execute different commands by collecting resistance changes induced by finger touches (Supplementary Fig. 35). We demonstrated the real-time gameplay of Tetris, where the pixels of the PeACEL array exhibit instantaneous responsivity on actuating various sensor keys (Fig. 5d and Supplementary Video 1). Passive matrix addressing could further increase the pixel resolution (Supplementary Fig. 36).

The integration of a flexible display with multifunctional electronics, encompassing temperature, electroencephalography, electrocardiography, electromyography and photoplethysmography sensors, enables the visual detection of physiological signals[39–42]. Real-time temperature monitoring furnishes valuable physiological data for pre-emptive intervention, which bears considerable importance for clinical and personalized medicine[43]. We developed a thin, deformable and waterproof visual temperature-monitoring system with a self-adhesive and conformal contact to the skin by integrating a micro temperature sensor and multicolour PeACEL devices (Supplementary Figs. 37 and 38). The serpentine-featured micro temperature sensor displays a linear response coupled with high sensitivity, a wide working range and high reliability (Supplementary Fig. 39). The colour alterations of the PeACEL devices can serve as a smart visual indicator or warning signal for real-time health conditions (Supplementary Fig. 40). The demonstration reveals the multicolour display's prompt responsiveness to varying temperatures (Fig. 5e,f and Supplementary Video 2). Additionally, the negligible heat generation and minimal

https://doi.org/10.1038/s41566-024-01455-6

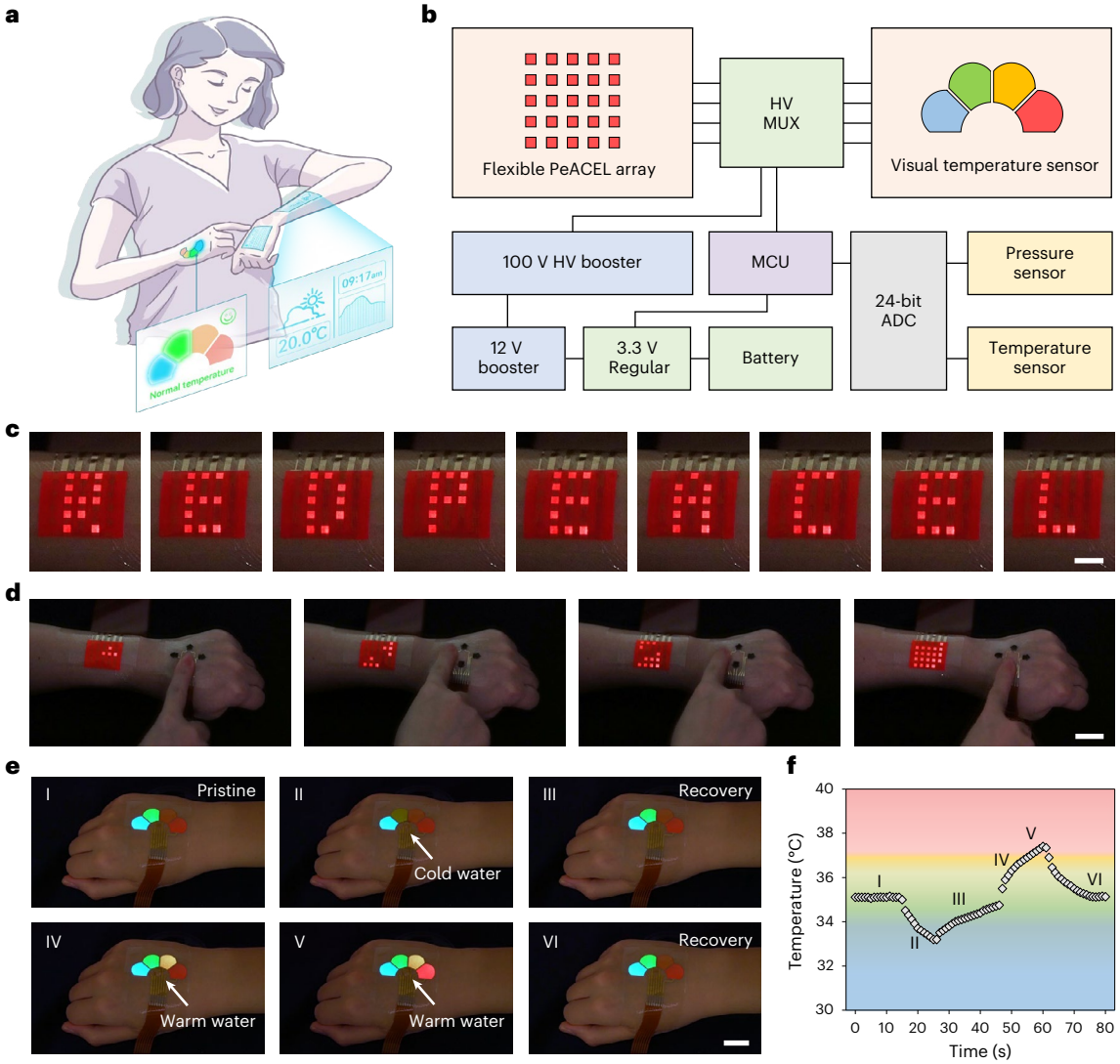

Fig. 5 | User-interactive skin display with a flexible PeACEL device. **a**, Conceptual image of the smart skin display. **b**, Block diagram of the integrated system. MCU, microcontroller unit; HV MUX, high-voltage multiplexer; ADC, analogue-to-digital converter. **c**, Demonstration of red-emitting PeACEL array laminated on the forearm. Scale bar, 1 cm. **d**, Demonstration of a dynamic interactive display. Scale bar, 2 cm. **e**, Demonstration of a visual temperature sensory system. Scale bar, 1 cm. **f**, Real-time temperature response in the testing period.

power consumption provide a guarantee for long-term uninterrupted operation (Supplementary Figs. 41–43).

Besides, due to their high adaptability to dynamic surfaces, ACEL devices hold great potential in soft robots, including dynamic information displays, smart camouflages and real-time object detection[6,9,44]. We also demonstrated a soft robotic system with visual sensory feedback functions, where the multicolour PeACEL device was equipped on a soft gripper to dynamically display its tactile information (Supplementary Figs. 44 and 45 and Supplementary Video 3). Thus, we predict that the multicolour PeACEL displays, exhibiting exceptional integrability, hold solid promise for emerging electronic wearables and soft robotics.

Conclusion

In this work, through ingenious material design and device fabrication, we develop a class of skin-integrated PeACEL devices possessing the merits of high colour purity, wide colour gamut, high brightness, low power consumption, long-term stability, remarkable flexibility and exceptional stretchability. The EL colour could be precisely modulated, encompassing nearly the entire visible spectrum, from blue to deep red. The luminance of the multicolour PeACEL devices is commensurate with that of the commercial blue ACEL device, with the green and red emissions surpassing those of their commercial counterparts. Consequently, we demonstrate user-interactive skin displays capable of instantaneous pattern or colour alterations, facilitated by integrating on-skin PeACEL devices and stimuli-responsive sensors with epidermal sensing properties. Such excellent performance of the PeACEL device is expected to significantly broaden the scope of the applications, particularly for multifunctional smart electronic skin, with potential utility in daily life.

Online content

Any methods, additional references, Nature Portfolio reporting summaries, source data, extended data, supplementary information, acknowledgements, peer review information; details of author contributions and competing interests; and statements of data and code availability are available at https://doi.org/10.1038/s41566-024-01455-6.

References

1. Yokota, T. et al. Ultraflexible organic photonic skin. *Sci. Adv.* **2**, e1501856 (2016).

2. Kim, D.-H. et al. Epidermal electronics. *Science* **333**, 838–843 (2011).
3. Morin, S. A. et al. Camouflage and display for soft machines. *Science* **337**, 828–832 (2012).
4. Zhao, X. et al. Self-powered user-interactive electronic skin for programmable touch operation platform. *Sci. Adv.* **6**, eaba4294 (2020).
5. Koo, J. H., Kim, D. C., Shim, H. J., Kim, T. H. & Kim, D. H. Flexible and stretchable smart display: materials, fabrication, device design, and system integration. *Adv. Funct. Mater.* **28**, 1801834 (2018).
6. Larson, C. et al. Highly stretchable electroluminescent skin for optical signaling and tactile sensing. *Science* **351**, 1071–1074 (2016).
7. Choi, H. W. et al. Smart textile lighting/display system with multifunctional fibre devices for large scale smart home and IoT applications. *Nat. Commun.* **13**, 814 (2022).
8. Sekitani, T. et al. Stretchable active-matrix organic light-emitting diode display using printable elastic conductors. *Nat. Mater.* **8**, 494–499 (2009).
9. Tan, Y. J. et al. A transparent, self-healing and high-κ dielectric for low-field-emission stretchable optoelectronics. *Nat. Mater.* **19**, 182–188 (2020).
10. Kim, T.-I. et al. Injectable, cellular-scale optoelectronics with applications for wireless optogenetics. *Science* **340**, 211–216 (2013).
11. Zhang, Z. et al. High-brightness all-polymer stretchable LED with charge-trapping dilution. *Nature* **603**, 624–630 (2022).
12. Zhao, M., Zhang, Q. & Xia, Z. Narrow-band emitters in LED backlights for liquid-crystal displays. *Mater. Today* **40**, 246–265 (2020).
13. Dai, X. et al. Solution-processed, high-performance light-emitting diodes based on quantum dots. *Nature* **515**, 96–99 (2014).
14. Stauffer, F. & Tybrandt, K. Bright stretchable alternating current electroluminescent displays based on high permittivity composites. *Adv. Mater.* **28**, 7200–7203 (2016).
15. Kim, J. S. et al. Ultra-bright, efficient and stable perovskite light-emitting diodes. *Nature* **611**, 688–694 (2022).
16. Kim, J.-H. & Park, J.-W. Intrinsically stretchable organic light-emitting diodes. *Sci. Adv.* **7**, eabd9715 (2021).
17. Han, T.-H. et al. Extremely efficient flexible organic light-emitting diodes with modified graphene anode. *Nat. Photon.* **6**, 105–110 (2012).
18. Liang, J., Li, L., Niu, X., Yu, Z. & Pei, Q. Elastomeric polymer light-emitting devices and displays. *Nat. Photon.* **7**, 817–824 (2013).
19. White, M. S. et al. Ultrathin, highly flexible and stretchable PLEDs. *Nat. Photon.* **7**, 811–816 (2013).
20. Shen, Y. et al. Rational interface engineering for efficient flexible perovskite light-emitting diodes. *ACS Nano* **14**, 6107–6116 (2020).
21. Choi, M. K. et al. Wearable red–green–blue quantum dot light-emitting diode array using high-resolution intaglio transfer printing. *Nat. Commun.* **6**, 7149 (2015).
22. Kwon, J. I. et al. Ultrahigh-resolution full-color perovskite nanocrystal patterning for ultrathin skin-attachable displays. *Sci. Adv.* **8**, eadd0697 (2022).
23. Shi, X. et al. Large-area display textiles integrated with functional systems. *Nature* **591**, 240–245 (2021).
24. Wang, L. et al. Application challenges in fiber and textile electronics. *Adv. Mater.* **32**, 1901971 (2020).
25. Park, J.-M. et al. Aromatic nonpolar organogels for efficient and stable perovskite green emitters. *Nat. Commun.* **11**, 4638 (2020).
26. Zhou, H. et al. Water passivation of perovskite nanocrystals enables air-stable intrinsically stretchable color-conversion layers for stretchable displays. *Adv. Mater.* **32**, 2001989 (2020).
27. Zhang, S. et al. Flexible alternating current electroluminescent devices integrated with high voltage triboelectric nanogenerators. *Nanoscale* **14**, 4244–4253 (2022).
28. Li, S. et al. Water-resistant perovskite nanodots enable robust two-photon lasing in aqueous environment. *Nat. Commun.* **11**, 1192 (2020).
29. Sun, C. et al. Efficient and stable white LEDs with silica-coated inorganic perovskite quantum dots. *Adv. Mater.* **28**, 10088–10094 (2016).
30. Deng, R., Wang, J., Chen, R., Huang, W. & Liu, X. Enabling Förster resonance energy transfer from large nanocrystals through energy migration. *J. Am. Chem. Soc.* **138**, 15972–15979 (2016).
31. Sun, Y. et al. Flexible alternating-current electroluminescence plunging to below 1 Hz frequency by triboelectrification. *Adv. Opt. Mater.* **10**, 2101918 (2022).
32. Wang, F. et al. Tuning upconversion through energy migration in core–shell nanoparticles. *Nat. Mater.* **10**, 968–973 (2011).
33. Jeong, S. M. et al. Bright, wind-driven white mechanoluminescence from zinc sulphide microparticles embedded in a polydimethylsiloxane elastomer. *Energy Environ. Sci.* **7**, 3338–3346 (2014).
34. Kim, E. H. et al. Organic light emitting board for dynamic interactive display. *Nat. Commun.* **8**, 14964 (2017).
35. Kim, E. H. et al. Interactive skin display with epidermal stimuli electrode. *Adv. Sci.* **6**, 1802351 (2019).
36. Zhao, Y. et al. Bioinspired multifunctional photonic-electronic smart skin for ultrasensitive health monitoring, for visual and self-powered sensing. *Adv. Mater.* **33**, 2102332 (2021).
37. Lee, S. W. et al. 3D motion tracking display enabled by magneto-interactive electroluminescence. *Nat. Commun.* **11**, 6072 (2020).
38. Wang, C. et al. User-interactive electronic skin for instantaneous pressure visualization. *Nat. Mater.* **12**, 899–904 (2013).
39. Lee, Y. et al. Standalone real-time health monitoring patch based on a stretchable organic optoelectronic system. *Sci. Adv.* **7**, eabg9180 (2021).
40. Tan, P. et al. Solution-processable, soft, self-adhesive, and conductive polymer composites for soft electronics. *Nat. Commun.* **13**, 358 (2022).
41. Zhang, L. et al. Fully organic compliant dry electrodes self-adhesive to skin for long-term motion-robust epidermal biopotential monitoring. *Nat. Commun.* **11**, 4683 (2020).
42. Lee, G.-H. et al. Rapid meniscus-guided printing of stable semi-solid-state liquid metal microgranular-particle for soft electronics. *Nat. Commun.* **13**, 2643 (2022).
43. Webb, R. C. et al. Ultrathin conformal devices for precise and continuous thermal characterization of human skin. *Nat. Mater.* **12**, 938–944 (2013).
44. Zhang, P. et al. Integrated 3D printing of flexible electroluminescent devices and soft robots. *Nat. Mater.* **13**, 4775 (2022).

Publisher's note Springer Nature remains neutral with regard to jurisdictional claims in published maps and institutional affiliations.

Open Access This article is licensed under a Creative Commons Attribution 4.0 International License, which permits use, sharing, adaptation, distribution and reproduction in any medium or format, as long as you give appropriate credit to the original author(s) and the source, provide a link to the Creative Commons licence, and indicate if changes were made. The images or other third party material in this article are included in the article's Creative Commons licence, unless indicated otherwise in a credit line to the material. If material is not included in the article's Creative Commons licence and your intended use is not permitted by statutory regulation or exceeds the permitted use, you will need to obtain permission directly from the copyright holder. To view a copy of this licence, visit http://creativecommons.org/licenses/by/4.0/.

© The Author(s) 2024

Methods

Materials

Caesium carbonate (Cs_2CO_3, 99.0%), oleic acid (OA, 90.0%), octadecene (90.0%), APTES (98.0%), trioctylphosphine (99.0%), lead chloride ($PbCl_2$, 99.0%), lead bromide ($PbBr_2$, 99.0%), lead iodide (PbI_2, 99.0%), toluene (AR), anisole (99.7%), octadecyltrichlorosilane (OTS, 95.0%) and methyl acetate (98.0%) were purchased from Sigma; PDMS (SYLGARD 184 silicone elastomer) was purchased from Dow Corning; Ecoflex 00-30 was purchased from Smooth-On; SEBS was purchased from Kraton; photoresist (PR; AZ 5214) was purchased from AZ Electronic Materials; and ZnS powders were purchased from Shanghai KPT. AgNWs were purchased from XFNANO. All the materials were used without further purification.

Synthesis of $CsPbX_3$ PeNPs

Here 0.4 g Cs_2CO_3, 15.00 ml octadecene, and 1.76 ml OA were loaded into a 100.00 ml three-necked flask under stirring and dried for 1 h at 120 °C under atmospheric conditions. The Cs-oleate precursor solution was obtained on complete dissolution. For the synthesis of $CsPbX_3$ PeNPs, a 50 ml three-necked flask was loaded with 0.376 mmol PbX_2 and 10 ml octadecene, which were dried for 1 h at 120 °C under atmospheric conditions. Subsequently, 1 ml OA and 1 ml APTES were slowly injected into the flask under stirring until the solution became clear. The temperature was increased to 140–180 °C, and 0.8 ml Cs-OA precursor solution was swiftly injected. After 5 s, the mixture solution was cooled down to room temperature using an ice-water bath. The $CsPbX_3$ PeNPs were washed with ethyl acetate and redispersed in 2 ml toluene for further use. For synthesizing $CsPbBr_2Cl$ PeNPs, 1 ml trioctylphosphine was used for the solubilization of lead chloride.

Synthesis of PeZS phosphors

Here 0.8 g ZnS phosphors were mixed with 2 ml PeNPs solution in a 10 ml vial and stirred vigorously. After 24 h, 10 µl APTES was added to the resultant solution. Then, the vial was opened to air and stirred for 6 h for hydrolysis. The precipitate was collected using centrifugation and washed with toluene to remove the excess APTES and OA. The PeZS phosphors were obtained after drying under a vacuum for 24 h.

Fabrication of rigid PeACEL devices

Indium-tin-oxide-coated glass substrates underwent sonication cleaning using detergent, acetone, deionized water and isopropanol, followed by a 15 min exposure to an ultraviolet (UV)–ozone environment. The mixture of PeZS phosphors, $BaTiO_3$ powders and PDMS (10:1) in a weight ratio of 3:1:1 was blade coated on indium tin oxide glass and dried at room temperature. Then, the silver paste electrode was applied to the surface of the EML. For the fabrication of patterned rigid PeACEL devices, a laser (wavelength, 365 nm; pulse energy, 47 µJ; frequency, 75 kHz; mark speed, 350 mm s^{-1}) was employed to cut the single-sided tape into the desired pattern, serving as a template for silver paste.

Fabrication of stretchable PeACEL devices using AgNWs

The stretchable PeACEL device comprises five consecutive layers, including SEBS substrate, AgNWs, EML, AgNWs and SEBS encapsulation layer. SEBS (3 g) elastomer was dissolved in a 5 ml toluene and 5 ml anisole mixture. The SEBS solution was spin coated (1,000 r.p.m., 10 s) on OTS-modified glass and dried at 80 °C for 30 min. The SEBS film was subsequently detached from the glass substrate and fixed on the linear translation stage. Before use, the AgNW solution was diluted in isopropanol. The AgNW solution was deposited on the pre-strained SEBS substrate by a spray gun, and then the bottom stretchable electrode was affixed to the OTS-modified glass substrate. The mixture of PeZS phosphors and SEBS solution with a weight ratio of 1:1 was blade coated on the bottom stretchable electrode and dried at room temperature. The top AgNW electrode was deposited on the pre-strained composite film using the spray gun. The composite film was positioned against the OTS-modified glass substrate, and the SEBS solution was blade coated on the surface to package the top electrode.

Fabrication of stretchable red PeACEL device using hydrogels

Here 8 M LiCl solution was prepared by dissolving 13.57 g LiCl in 40 ml deionized water. The solution was then combined with 5.69 g acrylamide and 807 mg polyacrylamide, and the mixture was subjected to continuous stirring at 60 °C for 4 h. Then, 20 mg *N*,*N*′-methylenebisacrylamide and 91 mg Irgacure 1173 were introduced into the mixture solution. After stirring overnight, the well-mixed gel was moulded into a Teflon mould and subjected to UV radiation for 5 min. The EML layer was created by combining the red PeZS phosphors and SEBS solution, which was then blade coated onto the OTS-modified glass substrate and left to dry at ambient temperature. The stretchable, hydrogel-based PeACEL device was assembled by encapsulating the EML layer between two hydrogel electrodes and SEBS films.

Fabrication of patterned and flexible PeACEL devices

The detailed fabrication procedure is depicted in Supplementary Fig. 46. The glass substrates were first cleaned and modified. Then, the SEBS solution was spin coated at 2,000 r.p.m. for 30 s and baked on a hotplate at 80 °C for 30 min. To obtain tailored patterns, commercial 50-µm-thick polyethylene terephthalate (PET) films that had been ablated by laser were used as masks. The patterned PET films were cleaned with acetone and deionized water, dried under a nitrogen flow and modified by OTS. Next, the diluted AgNW solution was deposited onto the mask-defined area of the SEBS film by a spray gun, followed by drying without annealing. The EML was prepared by blade coating the mixture of SEBS/PeZS with a scraper blade. To preserve the optimal performance of PeZS phosphors, no annealing was used in the subsequent steps. After placing the patterned PET mask on the EML, the diluted AgNW solution was spray coated as the top electrode. The mask was then removed, and the SEBS solution was spin coated (2,000 r.p.m., 30 s) as the encapsulation layer. Finally, the patterned PeACEL devices were peeled off from the glass substrate.

Fabrication of PeACEL array

The detailed fabrication process is shown in Supplementary Fig. 47. PDMS (10:1) was spin coated on the cleaned glass at 500 r.p.m. for 30 s and baked on a hotplate at 80 °C for 10 min. Afterwards, a 25-µm-thick polyimide (PI) film was laminated on the PDMS. The designed array pattern was directly cut using a laser system. Next, a layer of Au with a thickness of 100 nm was deposited on the PI layer by electron-beam evaporation (E-Beam, EBS-500F, Junsun). Following the removal of excess PI/Au, the array PI/Au pattern (named L1) was transferred by a water-soluble tape (WST). Supplementary Fig. 48 presents the detailed mechanical pattern design of the Au electrodes.

The SEBS solution was spin coated onto the OTS-modified glass substrate at 2,000 r.p.m. for 30 s and annealed at 80 °C for 30 min. The composite film L1 was laminated on the SEBS layer, and the WST was removed with water. The patterned EML was mounted by blade coating the mixture of SEBS/PeZS with a PET mask. Then, the mask was removed and the EML was dried at room temperature. Subsequently, the OTS-modified mask was laminated on the EML, and the AgNW solution was spray coated as the top electrode. After removing the mask, the SEBS solution was spin coated on the AgNWs at 2,000 r.p.m. for 30 s. The PeACEL array device could be peeled off after thorough drying. This PeACEL array device consists of 25 pixels, each with an area of 2.5 mm × 2.5 mm and a gap of 2.5 mm. Using the same method, an ultrasmall PeACEL array of 10 × 10 was fabricated. This smaller array consists of 100 pixels over an area of 1 cm × 1 cm. Each pixel has an area of 0.5 mm × 0.5 mm with a gap of 0.5 mm.

Fabrication of tactile sensor

The detailed fabrication process consists of five steps (Supplementary Fig. 49).

Step 1: fabrication began with the spin coating of PDMS (10:1) on a cleaned glass substrate at 500 r.p.m. for 30 s, followed by baking on a hotplate at 80 °C for 10 min. Subsequently, a PI film (25 μm) was laminated onto the PDMS layer. A laser was used to pattern the PI film by the direct-write method. Next, a layer of 100 nm Au was deposited onto the PI layer using electron-beam evaporation. After removing the residual portion, Au interdigitated electrode can be obtained. The detailed parameters of the interdigitated electrode are shown in Supplementary Fig. 50. The interdigitated electrode was picked up by WST and named L1.

Step 2: the flexible substrate was prepared by spin coating a SEBS solution onto the OTS-modified glass substrate at 2,000 r.p.m. for 30 s and annealed at 80 °C for 30 min. To transfer the interdigitated electrode to the SEBS layer, composite film L1 was laminated on the SEBS layer and the WST was removed. The resulting composite film was named L2.

Step 3: PDMS (10:1) was spin coated on the cleaned glass substrate and baked at 80 °C for 10 min. A commercial PET film was laminated on the PDMS layer and patterned using laser cutting. Then, the excess PET was carefully removed, and the designed pattern was transferred using the WST, named L3. The composite film L3 was laminated onto composite film L2, and the WST was removed with water, yielding composite film L4.

Step 4: LIG was prepared as the other electrode. PMMA (20 mg ml^{-1}, dissolved in an anisole solvent) was spin coated (2,000 r.p.m., 30 s) on a cleaned glass substrate as a sacrificial layer, and annealed at 200 °C for 30 min. A PI film (75 μm) was laminated on the PMMA layer. The PI was directly converted to the LIG electrode using a CO_2 laser with a wavelength of 1,064 nm. The non-patterned PI was removed, and the glass substrate with LIG was immersed in acetone to dissolve the PMMA. To preserve the integrity of LIG, a layer of PR was mounted by spin coating (3,000 r.p.m., 20 s). The LIG electrode was transferred by WST after removing the residual PR, resulting in composite film L5.

Step 5: a layer of PDMS was mounted on the cleaned glass substrate by spin coating PDMS (10:1) at 500 r.p.m. for 30 s, and baked on a hotplate at 80 °C for 10 min. Then, OTS double-sided-modified PET film (50 μm) was laminated on the PDMS layer. Next, a SEBS solution was spin coated (2,000 r.p.m., 30 s) on the PET film and annealed at 80 °C for 30 min. Composite film L5 was laminated on the SEBS layer to transfer the patterned LIG. A cotton swab soaked in acetone was used to remove the residual PR on the patterned LIG by gentle wiping. The PET/SEBS/LIG was peeled off from glass/PDMS and it was named L6. To fabricate the tactile sensor, composite L6 was carefully laminated onto composite L4 to align the two electrodes.

Fabrication of visual temperature-sensing system

The fabrication process for the visual temperature-sensing system shares similarities with the PeACEL array manufacturing. This device integrated the temperature sensor and PeACEL device. Initially, a layer of PDMS was mounted on a cleaned glass by spin coating at 500 r.p.m. for 30 s. Subsequently, the PI film (25 μm) was laminated on cured PDMS. A laser was exploited to carve the PI film into the designed pattern. Following this, E-Beam was used to deposit 100 nm Au on the PI layer. The detailed parameters of the pattern are presented in Supplementary Fig. 51. Four-petal-like PI/Au was used as the bottom electrode for EL devices, whereas the serpentine-structured PI/Au pattern in the centre served as the temperature sensor.

To prepare the soft substrate, the SEBS solution was spin coated (2,000 r.p.m., 30 s) on the OTS-modified glass substrate and dried at 80 °C for 30 min. Next, the patterned PI/Au was laminated on the SEBS layer and the WST was removed with water. To visualize the temperature variations, blue-, green-, yellow- and red-emitting PeZS phosphors were mixed with the SEBS solution, respectively. These mixtures of SEBS/PeZS were sequentially coated in the desired locations through various PET masks (50 μm). The patterned top electrode was prepared by spray coating an AgNW solution with an OTS-modified mask. The device was encapsulated with a layer of SEBS. Last, a flexible visual temperature-sensing device was achieved on detachment from the glass substrate.

Fabrication of the soft robot

The soft pneumatic robot comprises a top chamber layer, bottom layer and actuator-tubing connector. Initially, 3D-printed moulds were manufactured using a fused deposition modelling 3D printer (Bambu Lab). Ecoflex 00-30 (1:1) was poured into the 3D-printed moulds; following the degassing and curing processes, the pneumatic chamber layer and bottom layer were obtained. The flexible PI/Cu circuits were patterned using laser cutting and were subsequently transferred onto the bottom layer. The LIG prepared following the aforementioned preparation method was transferred to the PI/Cu circuits. The circuits and LIG were encapsulated using Ecoflex 00-30. The assembled pneumatically actuated soft robot was constructed by integrating the top chamber, bottom layer and actuator-tubing connector.

The PeACEL device comprises PDMS, AgNW electrodes and EML. PDMS was spin coated (900 r.p.m., 30 s) onto an OTS-modified glass substrate and dried at 80 °C for 30 min. The patterned PI/Cu, serving as the connector for the AgNW electrode and power source, was transferred onto the PDMS substrate. An OTS-modified mask was laminated on the substrate, followed by spray coating an AgNW solution to develop the bottom electrode. To prepare the patterned EML, a blend of PeZS and PDMS was blade coated on the surface of the bottom electrode using an OTS-modified mask. After curing, the AgNW solution was spray coated to form the top electrode. Post the lead-out of the electrode from PI/Cu by welding the metal wire, the device was encapsulated by spin coating PDMS. Finally, the PeACEL device was integrated into the soft pneumatic robot.

Materials characterization

Steady-state photoluminescence spectra were assessed by a Hitachi F-4600 fluorescence spectrophotometer. Time-resolved photoluminescence was recorded using an Edinburgh FLS1000 with a 375 nm laser. The TEM images were collected through an FEI/Philips Tecnai 12 BioTWIN TEM instrument. Scanning electron microscopy images were captured through a JEOL JSM IT500 scanning electron microscope. The optical transmittance spectra and UV–visible spectra were measured with a Hitachi UH4150 UV-VIS-NIR spectrophotometer. Fourier transform infrared spectra were collected by a PerkinElmer spectrometer in the range of 4,000–400 cm^{-1}. X-ray diffraction profiles were acquired on a Bruker D2 phaser XE-T X-ray diffractometer system using Cu Kα radiation (λ = 1.5406 Å).

Device measurement

The PeACEL device was powered by a high-voltage amplifier (Trek Model 2210) coupled with a dual-output function generator (Rigol DG811). The EL spectra were detected by a Maya2000 Pro spectrometer (Ocean Optics). A CS-200 Chroma Meter (Konica Minolta) was employed to measure the luminance of the EL device. The stretching test of the stretchable PeACEL device was performed on a linear translation stage. To quantify the turn-on delay of the PeACEL device, a photodiode (LSSPD-2.5) was employed to detect the light signal emitted by a red-emitting PeACEL device. PowerLab data acquisition hardware was used to record both driving signal and detected light signal.

Calculation of the power consumption of a PeACEL unit

As shown in Supplementary Fig. 43, a test circuit was employed to measure the power consumption of PeACEL units, at an a.c. frequency of 1 kHz. The voltages V_A and V_{BC} were first measured by an oscilloscope (Rigol DS1054). The current across resistors 2 and 3 was calculated as follows.

$$I_1 = V_A/R_1 \quad (1)$$

$$I_2 = V_{BC}/R_3 = V_{AB}/R_2 \quad (2)$$

According to equation (1), V_{AC} was calculated as follows.

$$V_{AC} = V_{AB} + V_{BC} = I_2 \times (R_2 + R_3) \quad (3)$$

The total power of the three resistors was

$$P_{resistor} = {I_1}^2 R_1 + {I_2}^2 R_2 + {I_3}^2 R_3. \quad (4)$$

The total power of the test circuit was calculated as

$$P_{total} = I_1 V_{AC} \cos\theta, \quad (5)$$

where θ represents the phase shift between the current and voltage waveforms across the test circuit and was measured as 72° by the oscilloscope. Hence, the power consumption of the PeACEL unit was given by

$$P_{PeACEL} = P_{total} - P_{resistor}. \quad (6)$$

Data availability

All data supporting the results of this study are available in the Article and its Supplementary Information. Source data are provided with this paper.

Acknowledgements

The work described in this paper was substantially supported by a fellowship award (project no. CityU RFS2021-1S03) and a general research fund (project no. CityU 11211922) from the Research Grants Council of the Hong Kong Special Administrative Region, China.

Author contributions

F.C. and F.W. conceived and designed this research project. F.C. and B.Z. performed the experiments on the materials synthesis, device design and fabrication. F.C., Y. Gao, X.W., J.Z. and X.Y. performed the system integration and test. Q.Z. performed the biocompatibility test. F.C., W.Z., Y. Guo, X.Z. and Z.X. performed the materials characterization and data analysis. F.C., B.Z., Y. Gao, X.Y. and F.W. discussed the data and wrote the manuscript. All authors contributed to the analysis of this manuscript.

Competing interests

The authors declare no competing interests.

Additional information

Supplementary information The online version contains supplementary material available at https://doi.org/10.1038/s41566-024-01455-6.

Correspondence and requests for materials should be addressed to Xinge Yu or Feng Wang.

Peer review information *Nature Photonics* thanks Chuan Wang, Tae-Woo Lee and the other, anonymous, reviewer(s) for their contribution to the peer review of this work.

Reprints and permissions information is available at www.nature.com/reprints.